Gas-particle partitioning of polyol tracers at a suburban site in Nanjing, east China: Increased partitioning to the particle phase

Chao Qin[1], Yafeng Gou[2], Yuhang Wang[3], Yuhao Mao[2], Hong Liao[2], Qin'geng Wang[4], Mingjie Xie[2,*]

[1]Colleges of Resources and Environmental Sciences, Nanjing Agricultural University, Nanjing 210095, China

[2]Collaborative Innovation Center of Atmospheric Environment and Equipment Technology, Jiangsu Key Laboratory of Atmospheric Environment Monitoring and Pollution Control, School of Environmental Science and Engineering, Nanjing University of Information Science & Technology, 219 Ningliu Road, Nanjing 210044, China

[3]School of Earth and Atmospheric Sciences, Georgia Institute of Technology, Atlanta, GA 30332

[4]State Key Laboratory of Pollution Control and Resources Reuse, School of the Environment, Nanjing University, Nanjing 210023, China

*Corresponding to:

Mingjie Xie (mingjie.xie@nuist.edu.cn; mingjie.xie@colorado.edu);

Tel: +86-18851903788l; Fax: +86-25-58731051;

Mailing address: 219 Ningliu Road, Nanjing, Jiangsu, 210044, China

Abstract

Gas-particle partitioning of water-soluble organic compounds plays a significant role in influencing the formation, transport, and lifetime of organic aerosols in the atmosphere, but is poorly characterized. In this work, gas- and particle-phase concentrations of isoprene oxidation products (C5-alkene triols and 2-methylterols), levoglucosan, and sugar polyols were measured simultaneously at a suburban site of the western Yangtze River Delta in east China. All target polyols were primarily distributed into the particle phase (85.9–99.8%). Given the uncertainties in measurements and vapor pressure predictions, a dependence of particle-phase fractions on vapor pressures cannot be determined. To explore the impact of aerosol liquid water on gas-particle partitioning of polyol tracers, three partitioning schemes (*Cases 1-3*) were proposed based on equilibriums of gas versus organic and aqueous phases in aerosols. If particulate organic matter (OM) is presumed as the only absorbing phase (*Case 1*), the measurement-based absorptive partitioning coefficients ($K^m_{p,OM}$) of isoprene oxidation products and levoglucosan were more than 10 times greater than predicted values ($K^t_{p,OM}$). The agreement between $K^m_{p,OM}$ and $K^t_{p,OM}$ was substantially improved when solubility in a separate aqueous phase was included, whenever water-soluble and water-insoluble OM partitioned into separate (*Case 2*) or single (*Case 3*) liquid phases, suggesting that the partitioning of polyol tracers into the aqueous phase in aerosols should not be ignored. The measurement-based effective Henry's law coefficients ($K^m_{H,e}$) of polyol tracers were orders of magnitude higher than their predicted values in pure water ($K^t_{H,w}$). Due to the moderate correlations between log ($K^m_{H,e}/K^t_{H,w}$) and molality of sulfate ions, the gap between $K^m_{H,e}$ and $K^t_{H,w}$ of polyol tracers could not be fully parameterized by the equation defining

54 "salting-in" effects, and might be ascribed to mechanisms of reactive uptake, aqueous

55 phase reaction, "like-dissolves-like" principle, etc. These study results also partly

56 reveals the discrepancy between observation and modeling of organic aerosols.

57

58

59

60

61

62

63

64

65

66

67

68

69

70

71

72

73

74

75

76

1 Introduction

The water-soluble organic carbon (WSOC) in ambient aerosols can account for 20-80% of particulate organic matter (OM) based on carbon mass (Saxena and Hildemann, 1996; Kondo et al., 2007). Field studies on the hygroscopic growth and cloud condensation nucleus (CCN) activity of aerosol extracts indicated that WSOC contributed significantly to aerosol hygroscopicity, and modified the hydration behavior of inorganic species (e.g., sulfate, nitrate, and ammonium; Hallar et al., 2013; Taylor et al., 2017). Thus, WSOC plays an important role in changing radiative and cloud nucleating properties of atmospheric particles. Particulate WSOC is a complex mixture of polar organic compounds containing oxygenated functional groups (e.g., hydroxyl, carboxyl, and carbonyl groups), among which a list of organic compounds with multiple hydroxyl (polyols) groups have been identified using gas chromatography -mass spectrometry (GC-MS) and linked with specific emission sources. For example, C5-alkene triols and 2-methyltetrols are isoprene oxidation products (Claeys et al., 2004; Wang et al., 2005; Surratt et al., 2006); levoglucosan is a typical pyrolysis product of cellulose (Simoneit et al., 1999); primary saccharides (e.g., fructose and glucose) and saccharide polyols (e.g., arabitol and mannitol) are commonly associated with soil microbiota and fungal spores, respectively (Simoneit et al., 2004; Bauer et al., 2008).

To quantify the sources contributing to WSOC, concentrations of individual organic tracers are often used as inputs for receptor-based modeling (Zhang et al., 2009; Hu et al., 2010). Due to the influences of gas-particle partitioning on source apportionment, Xie et al. (2013, 2014c) suggested the involvement of gas-phase concentrations of organic makers through theoretical prediction or field measurements.

The equilibrium absorptive partitioning theory outlined by Pankow (1994a, b) and laboratory measurements of secondary organic aerosol (SOA) yields (Odum et al., 1996) have been widely applied to predict SOA formation in traditional modeling studies (Heald et al., 2005; Volkamer et al., 2006; Hodzic et al., 2010). In addition to absorptive partitioning to particulate OM after the formation of oxygenated organic compounds in gas phase, other formation pathways (e.g., reactive uptake) have been identified and are responsible for the large discrepancy between modeled and observed SOA loadings (Jang et al., 2002; Kroll et al., 2005; Perraud et al., 2012). Unlike non-polar species (e.g., *n*-alkanes, polycyclic aromatic hydrocarbons) and alkanoic acids that are well simulated (Simcik et al., 1998; Xie et al., 2014a; Yatavelli et al., 2014; Isaacman-VanWertz et al., 2016), particle-phase concentrations of carbonyls were underestimated by several orders of magnitude when particulate OM is presumed as the only absorbing phase assuming ideal mixing condition (Healy et al., 2008; Kampf et al., 2013; Shen et al., 2018). Zhao et al. (2013) observed a positive dependence of particle-phase pinonaldehyde on relative humidity (RH, %), and inferred that aerosol water played a role in the formation of pinonaldehyde in the atmosphere. However, very few studies have been performed on the measurement of gaseous polyols (Xie et al., 2014b; Isaacman-VanWertz et al., 2016), and their gas-particle partitioning were poorly understood.

Henry's law can describe the uptake of a compound into a liquid, highly dilute solution (e.g., cloud droplets) in the atmosphere (Ip et al., 2009; Compernolle and Müller, 2014a). Aerosol water is also a major component of atmospheric particles, and accounts for 40% by volume at 50% RH in Europe (Tsyro, 2005). But the bulk aerosol solution is highly concentrated with inorganic ions and WSOC. An effective

125 Henry's law coefficient ($K_{H,e}$, mol m^{-3} atm^{-1}) can be used to account for the measured

126 partitioning between the gas phase and aerosol liquid water (Volkamer et al., 2009).

127 Both laboratory and field studies observed enhanced $K_{H,e}$ of carbonyl compounds with

128 inorganic salt concentrations (in mol kg^{-1} aerosol liquid water content, ALWC; Kampf

129 et al., 2013; Waxman et al., 2015; Shen et al., 2018). This "salting-in" effect

130 (Setschenow, 1889) is not mechanistically understood, and might be linked with the

131 hydrophilic interactions (e.g., hydrogen bonding) between polar organic compounds

132 and inorganic ions leading to an increase of entropy or decrease of Gibbs free energy

133 (Almeida et al., 1983; Waxman et al., 2015). Polyol tracers are highly water-soluble

134 and their gas-particle partitioning is very likely driven by the aqueous phase

135 containing substantial ionic species in ambient aerosols. In the Southeastern US, the

136 particle-phase fraction (*F*%) of WSOC is highly dependent on RH and ALWC

137 (Hennigan et al., 2009).

138   In the present study, polyols related to specific emission sources in gaseous and

139 particle phases were measured concurrently in northern Nanjing, China. The sampling

140 and chemical analysis were performed in a similar manner as Xie et al. (2014b), while

141 an additional step was added prior to GC-MS analysis to clean the extracts of gaseous

142 samples. To explore the roles of aerosol liquid water on gas-particle partitioning of

143 polyol tracers, three modes (*Cases 1-3*) were proposed based on equilibriums between

144 gas and liquid aerosol phases, and the measurement-based and predicted partitioning

145 coefficients were compared across individual cases. This work tends to explain the

146 gas-particle partitioning of polyols at a suburban site in eastern China, where the

147 estimated average mass concentration of aerosol liquid water is close to 20 µg m^{-3}

148 (Yang et al., 2021).

2 Methods

2.1 Field Sampling

Details of the sampling information were provided in Yang et al. (2021). Briefly, ambient air was sampled on the rooftop of a seven-story library building located in Nanjing University of Information Science and Technology (NUIST 32.21 $^{\circ}$N, 118.71 $^{\circ}$E), a suburban site in the western Yangtze River Delta of east China. A medium volume sampler (PM-PUF-300, Mingye Environmental, Gugangzhou, China) equipped with a 2.5 µm cut impactor was configured to collect particulate matter with aerodynamic diameter less than 2.5 µm ($PM_{2.5}$) and gaseous organic compounds at a flow rate of 300 L min^{-1}. After the impactor, the sampled air flowed through a filter pack containing two stacked pre-baked (550 $^{\circ}$C, 4 h) quartz filters (20.3 cm $\times$ 12.6 cm, Munktell Filter AB, Sweden) and a polyurethane foam (PUF, 65 mm diameter $\times$ 37.5 mm length) cartridge in series. The top quartz filter (Q_f) in the filter pack was loaded with $PM_{2.5}$; gaseous organic compounds adsorbed on the backup quartz filter (Q_b) were determined to evaluate sampling artifacts; and the PUF cartridge was used for the sampling of gaseous polyols. Filter and PUF samples were collected every sixth day during daytime (8:00 AM – 7:00 PM) and night time (7:00 PM – 7:00 AM next day), respectively, from 09/28/2018 to 09/28/2019. Collection efficiency of gaseous polyols were examined by performing breakthrough experiments using two PUF plugs during nine sampling intervals. Prior to sampling, PUF adsorbents were cleaned and dried in the same way as Xie et al. (2014b). Field blank filter and PUF materials were collected every 10th sample for contamination adjustment. Filter and PUF samples were sealed in prebaked aluminum foil and glass jars, respectively, at – 20 $^{\circ}$C until analysis.

2.2 Chemical Analysis

Bulk speciation. The accumulated $PM_{2.5}$ mass and bulk components including water soluble ions (NH_4^+, SO_4^{2-}, NO_3^-, Ca^{2+}, Mg^{2+}, and K^+), organic (OC) and elemental carbon (EC), and WSOC were measured for each filter sample. Their final concentrations were determined by subtracting measurement results of Q_b from those of Q_f. Concentrations of aerosol liquid water were predicted by ISORROPIA II model using ambient temperature, RH, and concentration data of NH_4^+, SO_4^{2-}, and NO_3^- under the metastable state. The estimated water content contributed by hygroscopic WSOC was relatively small (< 1 μg m^{-3}) and not accounted for in this work (Text S1 of supplementary information). Table S1 lists averages and ranges of ambient temperature, RH, measured $PM_{2.5}$ components, and predicted aerosol liquid water from Yang et al. (2021).

Polyols analysis. Details of the analysis method for gaseous and particulate polyols were provided in supplementary information (Text S2). Briefly, 1/8 of each filter sample was pre-spiked with deuterated internal standard and extracted ultrasonically twice for 15 min in 10–15 mL of methanol and methylene chloride mixture (1:1, v/v). After filtration, rotary evaporation, N_2 blown down to dryness, and reaction with 50 μL of N, O-bis(trimethylsilyl)trifluoroacetamide (BSTFA) containing 1% trimethylchlorosilane (TMCS) and 10 μL of pyridine, the derivatives of polyols were diluted to 400 μL using pure hexane for GC-MS analysis. Pre-spiked PUF samples were Soxhlet extracted using a mixture of 225 mL of methylene chloride and 25 mL of methanol, followed by the same procedures of filter sample pretreatment. Prior to GC-MS analysis, 50 μL of pure water was added to precipitate PUF impurities from the final extract. As shown in Figure S1e, all PUF residues are kept in aqueous phase

197 at the bottom of the vial, while the derivatives of polyol tracers are supposed to be

198 retained in the top clear hexane solution. An aliquot of 2 µL of the supernatant was

199 injected for GC-MS analysis under splitless mode, and an internal standard method

200 with a six-point calibration curve (0.05–5 ng µL^{-1}) was performed to quantify polyols

201 concentrations. In this work, isoprene SOA products, including three C5-alkene triols

202 (cis-2-methyl-1,3,4-trihydroxy-1-butene, 3-methyl-2,3,4-trihydroxy-1-butene, and

203 trans-2-methyl-1,3,4-trihydroxy-1-butene; abbreviated as C5-alkene 1, 2, and 3) and

204 two 2-methyltetrols (2-methylthreitol and 2-methylerythritol), were quantified using

205 meso-erythritol; other polyols were determined using authentic standards.

206   Analytical recoveries of target polyols were obtained by adding known amounts

207 of standards to blank sampling materials (quartz filter and PUF), followed by

208 extraction and instrumental analysis identically as ambient samples. Method detection

209 limits (MDL) of individual species were estimated as three times the standard

210 deviation of their concentrations determined from six injections of the lowest

211 calibration standard. Table S2 lists recovery and MDL values of authentic standard

212 compounds. Concentrations of polyols in field blank samples were measured and

213 subtracted from air samples if necessary. To obtain appropriate gas-particle

214 distribution of polyol tracers, their field-blank corrected concentrations in filter and

215 PUF samples were adjusted by recoveries. Final concentrations of individual polyols

216 in Q_f, Q_b, and PUF samples are summarized in Table S3.

217 *2.3 Data analysis*

218 **Gas-particle separation and breakthrough calculation.** Polyol tracers detected in

219 Q_b samples are contributed by both gaseous adsorption ("positive artifact") and

220 particle-phase evaporation from Q_f samples ("negative artifact"), but their relative

221 contributions are unknown. Xie et al. (2014b) adjusted particle- and gas-phase

222 concentrations of levoglucosan and 2-methyltetrol based on Q_b measurements in two

223 different ways. One assumed that Q_b values were completely attributed to gaseous

224 adsorption; the other presumed equal contributions from gaseous adsorption and Q_f

225 evaporation. However, negligible difference in gas-particle distribution was observed

226 due to the small Q_b values. In Table S3, concentrations of polyol tracers on Q_b are far

227 below those on Q_f, and it would be safe to presume equal positive and negative

228 artifacts. In this study, particle-phase concentrations of polyols were represented by Q_f

229 values, and the gas phase was calculated as the sum of Q_b and PUF measurements.

230   The sampling efficiency of target polyols were evaluated by collecting and

231 analyzing tandemly installed PUF plugs during nine sampling intervals. The

232 breakthrough of each polyol was calculated as

233     $$B = \frac{[\text{PUF}]_{\text{back}}}{[\text{PUF}]_{\text{front}} + [\text{PUF}]_{\text{backup}}} \times 100\% \qquad (1)$$

234 where B is the breakthrough of gaseous sampling, and [PUF] represents the

235 concentration of specific compound in front or backup PUF sample. A value of 33%

236 was typically used to indicate excessive breakthrough (Peters et al., 2000; Ahrens et

237 al., 2011).

238 **Calculations of partitioning coefficients**. Here, we defined three partitioning cases

239 to explore the influence of dissolution in aerosol liquid water on gas-particle

240 partitioning of polyol tracers in the atmosphere. *Case 1* presumes instantaneous

241 equilibrium between the gas phase and particulate OM based on the equilibrium

242 absorptive partitioning theory. In this case, particulate OM is assumed to be the only

243 absorbing phase and behave as an ideal solution. Then the absorptive gas-particle

244 partitioning coefficients ($K_{p,OM}$, m^3 μg^{-1}) were calculated from measurements ($K^m_{p,OM}$)

245   and predicted theoretically ($K^{\text{t}}_{\text{p,OM}}$) as follows (Pankow, 1994a, b; Liang and Pankow,

246   1996; Liang et al., 1997; Mader and Pankow, 2002)

247    $$K^{\text{m}}_{\text{p,OM}} = \frac{F/M_{\text{OM}}}{A} \qquad (2)$$

248    $$K^{\text{t}}_{\text{p,OM}} = \frac{RT}{10^6 \overline{\text{MW}}_{\text{OM}} \zeta_{\text{OM}} p^{\text{o}}_{\text{L}}} \qquad (3)$$

249   where M_{OM} denotes the mass concentration of absorptive organic matter (OM = OC $\times$

250   1.6; Turpin and Lim, 2001); F (ng m^{-3}) and A (ng m^{-3}) are particulate and gaseous

251   concentrations of individual polyols, respectively. In eq 3, R (m^3 atm K^{-1} mol^{-1}) and T

252   (K) are the ideal gas constant and ambient temperature; $\overline{\text{MW}}_{\text{OM}}$, average molecular

253   weight of absorptive OM, is set at 200 g mol^{-1} for all samples (Barsanti and Pankow,

254   2004; Williams et al., 2010); ζ_{OM} denotes the mole fraction scale activity coefficient,

255   and is presumed to be unity for all species in each sample; p^{o}_{L} (atm) is the vapor

256   pressure of each pure compound, and is predicted with several estimation tools and

257   adjusted for each sampling interval based on the average temperature (Text S3 and

258   Table S4).

259   Due to the influence of mixing state and water content in aerosols, several studies

260   modeled the gas-particle partitioning of oxygenated organic compounds by defining a

261   liquid-liquid phase separation (LLPS) in the aerosol (Zuend and Seinfeld, 2012; Pye

262   et al., 2018). The organic-inorganic interactions and changes of activity coefficients in

263   aqueous mixtures were fully considered as well. In this study, we proposed a

264   simplified LLPS partitioning mechanism (*Case 2*) in Figure 1. First, aerosol water and

265   water-insoluble OM (WIOM = OM − WSOC $\times$ 1.6) exist in two separate liquid

266   phases, and WSOC and inorganic ions are totally dissolved in the aqueous phase. The

267   distribution of polyol tracers between aqueous (F_{W}, ng m^{-3}) and WIOM (F_{WIOM}, ng m^{-}

268 ^{3}) phases is simply depicted by their octanol-water partition coefficients (K_{OW})

269 $$K_{OW} = \frac{F_{WIOM}/V_{WSIOM}}{F_w/V_w} = \frac{c_{WIOM}}{c_w} \qquad (4)$$

270 where V_{WIOM} and V_w are volumes (m^3) of WIOM and water in aerosols per cubic

271 meter air; c_{WIOM} and c_w are solution concentrations (ng m^{-3}) of polyols concentrations

272 in organic and aqueous phases; log K_{OW} values of target polyols were estimated using

273 the Estimation Programs Interface (EPI) Suite developed by the US Environmental

274 Protection Agency and Syracuse Research Corporation (Table S4; US EPA, 2012).

275 The density of organic matter and water (ρ_w) in aerosols are set at 1.4 and 1.0 g cm^{-3},

276 respectively (Isaacman-VanWertz et al., 2016; Taylor et al., 2017). Second, gas-phase

277 polyol tracers are in equilibrium with hydrophobic OM and the aqueous phase,

278 respectively

279 $$K_{p,WIOM}^m = \frac{F_{WIOM}/M_{WIOM}}{A} \qquad (5)$$

280 $$K_{H,e}^m = \frac{\frac{F_w}{M_i}}{\frac{A}{M_i} \times R \times T \times \frac{c_{ALW}}{\rho_w}} = \frac{\rho_w \times F_w}{A \times R \times T \times c_{ALW}} \qquad (6)$$

281 where $K_{H,e}^m$ (mol m^{-3} atm^{-1}) is the measurement-based effective Henry's law

282 coefficient; M_{WIOM} represents the mass concentration (μg m^{-3}) of WIOM; M_i (g mol^{-1})

283 is the molecular weight of specific compound; c_{ALW} (μg m^{-3}) is the mass

284 concentration of aerosol liquid water predicted using ISORROPIA II model. *Case 3* is

285 generally the same as *Case 2*, and the only difference is that water-soluble OM

286 (WSOM) and WIOM exist in a single organic phase. Here total particulate OM was

287 used instead of WIOM to assess the distribution of polyol tracers between aqueous

288 and organic phases, and calculate partitioning coefficients of gas vs. particulate

289 organic ($K_{p,OM}^m$) and aqueous ($K_{H,e}^m$) phases. Note that the polarity of particulate OM

290 phase in *Case 3* was expected to increase, then using K_{OW} to calculate the distribution

291 of polyols between organic and aqueous phases might lead to underestimated $K^m_{p,OM}$

292 and overestimated $K^m_{H,e}$. For comparison purposes, the Henry's law coefficient in

293 pure water at 25 °C ($K^*_{H,w}$) was estimated using EPI and SPARC (Hilal et al., 2008;

294 http://archemcalc.com/sparc-web/calc), respectively (Table S4), and was adjusted for

295 each sampling interval due to the changes in ambient temperature using van 't Hoff

296 equation (Text S4).

297 ***Uncertainty estimation.*** To obtain the uncertainty associated with the calculation of *F*%

298 and partitioning coefficients ($K^m_{p,OM}$ and $K^m_{H,e}$), measurement uncertainties of polyol

299 tracers in filter and PUF samples were estimated from their recoveries and

300 breakthrough for gaseous sampling. The root sum of squares (RSS) method was

301 applied to propagate uncertainties of gas and particle-phase concentrations for *F*%,

302 $K^m_{p,OM}$, and $K^m_{H,e}$ calculations. Details of the uncertainty estimation and propagation

303 methods were provided in Text S5, and the average relative uncertainties were

304 summarized in Table S5.

305 **3 Results and discussion**

306 *3.1 Method evaluation*

307 In our previous study, PUF/XAD-4 resin/PUF and PUF/XAD-7 resin/PUF

308 adsorbent sandwiches were tested for sampling gaseous 2-methyltetrols and

309 levoglucosan (Xie et al., 2014b). The results of breakthrough experiments suggested

310 that both the two sandwiched composites had high sampling efficiency (close to

311 100%). Moreover, individual parts of the two types of composites (top PUF, middle

312 XAD-4/XAD-7 resin, and backup PUF) were analyzed for 7 samples, and target

313 compounds were only detected in top PUF. It is therefore suitable to collect gaseous

314 2-methylterols and levoglucosan using PUF materials only.

Although PUF materials were pre-cleaned prior to sampling, a few short-chain polyurethanes or impurities could be dissolved during Soxhlet extraction of target compounds using the mixture of methanol and methylene chloride. These substances precipitated when sample extracts were concentrated (Figure S1a, b), and re-dissolved in BSTFA:TMCS/pyridine and hexane after the derivatization step (Figure S1c, d). In Xie et al. (2014b), an aliquot of 2 µL of the sample extract as shown in Figure S1d was injected for GC-MS analysis. Since the dissolved PUF materials did not vaporize at ~300 °C, the GC inlet liner had to be changed for cleaning every few samples. In this work, 50 µL of pure water was added to separate PUF materials from polyol derivatives in hexane solution. As shown in Figure S1e, all PUF residues were retained in the aqueous solution after phase separation. This pretreatment step was added for the analysis of gaseous samples to save time for changing and cleaning GC inlet liners. However, the revised method did not improve the recoveries of meso-erythritol and levoglucosan in PUF samples (Table S2) compared to those in Xie et al. (2014b). This is because the dissolved PUF materials should have an impact on the derivatization efficiency of polyol species, and future work is warranted to remove dissolved PUF materials in sample extracts before the derivatization step.

Measurement results of breakthrough samples and the resulting B values were shown in Figure S2. C5-alkene triols and 2-methyltetrols were mainly observed in summertime, and levoglucosan was only detected in three pairs of breakthrough samples. Their average B values ($< 33\%$) indicated no excessive breakthrough (Figure S2a-c), but were higher than those reported by Xie et al. (2014b). This might be ascribed to the greater face velocity (1.5 cm s^{-1}) for sampling gaseous polyols than that (0.61 cm s^{-1}) in our previous study. Due to the limit in sample number for

339 breakthrough tests and low detection rates, the dependence of breakthrough on

340 ambient temperature or OM loadings cannot be evaluated. The breakthrough of an

341 ideal sampling method is expected to be extremely low (e.g., <10%) and have no

342 dependence on ambient temperature, OM loadings, etc. Unlike fructose which had

343 low breakthrough (Figure S2d), glucose and mannitol had comparable concentrations

344 between front and backup PUF samples for several breakthrough experiments (Figure

345 S2e, f), indicating that PUF materials are not suitable for sampling gaseous glucose

346 and mannitol. Mannose and arabitol were not detected or had BDL values for

347 breakthrough samples, and their breakthrough was not provided. In the current work,

348 concentrations of polyol tracers in filter and PUF samples were all reported, but the

349 data of mannose, glucose, arabitol, and mannitol in PUF samples should be treated

350 with caution due to high breakthrough or the lack of valid breakthrough results.

351 *3.2 General description of measurement results*

352 Total ambient concentrations ($Q_f + Q_b$ + PUF) of individual polyols are depicted

353 using boxplots in Figure 2. Figure S3 presents temporal variations of total and Q_f

354 concentrations of individual polyols with daytime and night-time measurements

355 distinguished. In general, polyol tracers were predominantly observed on Q_f with

356 averages 1-3 orders of magnitude higher than those on Q_b and PUF (Table S3).

357 Levoglucosan had the highest average total concentration (66.1 $\pm$ 71.1 ng m^{-3}),

358 followed by fructose (15.0 $\pm$ 62.9 ng m^{-3}) and mannose (14.3 $\pm$ 31.3 ng m^{-3}). C5-

359 alkene triols and 2-methyltetrols are formed from isoprene epoxydiols (IEPOX) under

360 low NO$_X$ conditions (Surratt et al., 2010). All the five species on Q_b were more

361 frequently detected and had average concentrations 2-20 times higher than those in

362 PUF samples. While in Xie et al. (2014b), the sum of 2-methyltetrols in Q_b and

363   adsorbent samples were up to 2.7 times higher than those on Q_f in summer Denver, so

364   isoprene products are not similarly distributed between gas and aerosol phases across

365   different regions. Moreover, isoprene-derived polyols exhibited prominent elevations

366   in summer (Figure S3a-e), and their daytime concentrations ($2.02 \pm 3.73 - 10.5 \pm 29.3$

367   ng m^{-3}) were only slightly higher than those during night-time ($1.63 \pm 4.40 - 9.65 \pm$

368   32.7 ng m^{-3}). Previous field studies observed strong diurnal variations of isoprene

369   SOA tracers with peak concentrations from afternoon till midnight (Fu and Kawamura,

370   2011; Isaacman-VanWertz et al., 2016). Although no IEPOX will be generated from

371   the oxidation of isoprene by •OH and HO$_2$• after sunset, the formations of C5-alkene

372   triols and 2-methyltetrols might continue until pre-existing IEPOX is exhausted. In

373   this work, neither the daytime (8:00 AM–7:00 PM) or night-time (7:00 AM–7:00 AM

374   next day) sample covered the whole period when isoprene SOA tracers had peak

375   concentrations, and the strong diurnal variations of C5-alkene triols and 2-

376   methyltetrols were not captured.

377   Levoglucosan was more frequently detected but far less concentrated in PUF than

378   in Q_b samples. Its total concentrations were comparable to those in urban Denver

379   (average 65.3 ± 96.8 ng m^{-3}, range $2.48 - 478$ ng m^{-3}), where an average of ~20%

380   partitioned into the gas phase (Xie et al., 2014b). Due to the enhanced biomass

381   burning activities in cold periods for domestic heating at night, levoglucosan showed

382   a clear seasonal pattern (winter maxima and summer minima) and significant ($p =$

383   0.03) higher concentrations during night-time (Figure S3f). Sugars and sugar alcohols

384   are commonly linked with soil/dust resuspension and associated microbial activities

385   (Simoneit et al., 2004). They were frequently detected in Q_b samples with comparable

386   averages and ranges as those in PUF samples (Table S3). Total concentrations of

387   fructose and glucose were strongly ($r = 0.98$) correlated peaking in middle spring

388   (April 2019, Figure S3h, j), when Ca^{2+} on Q_f also reached its maxima of the year

389   (Yang et al., 2021), indicating an influence from soil/dust resuspension. Arabitol and

390   mannitol had identical seasonal pattern ($r = 0.89$) with elevated total concentrations

391   from May to October (Figure S3i, m), which might be attributed to high levels of

392   vegetation during growing seasons and autumn decomposition (Burshtein et al., 2011).

393   Multiple peaks of mannose concentrations were observed from spring to autumn,

394   suggesting a variety of contributing sources (e.g., microbial activity, vegetation).

395   Xylitol is likely derived from biomass burning in northern Nanjing due to its strong

396   correlation ($r = 0.89$) with levoglucosan.

397   *3.3 Gas- and particle-phase distributions*

398   As mentioned in sections 2.3, concentrations of particulate polyols were obtained

399   directly from Q_f measurements, and the gas phase was calculated as the sum of Q_b and

400   PUF values. Figure S4 shows the time series of gas-phase concentrations and particle-

401   phase fractions ($F\%$) of individual polyol tracers. The average $F\%$ values of measured

402   species are plotted against the logarithms of their liquid-state vapor pressures at 25 °C

403   ($p^{o,*}_L$) in Figure 3. Gas-phase C5-alkene triols and 2-methyltetrols had maximum

404   concentrations in summer and significant ($p < 0.05$) day-night variations (Figure S4),

405   while other polyols had extremely low concentrations in the gas phase with $F\%$

406   (average ± standard deviation) ranging from $94.2 \pm 8.02 - 99.8 \pm 1.21\%$. The average

407    $F\%$ values of 2-methyltetrols ($87.5 \pm 10.6\%$) and levoglucosan ($99.8 \pm 1.21\%$) were

408   greater than those in urban Denver (50–80%; Xie et al., 2014b), where the average

409   sampling temperature (12.5 ± 10.1 °C) was much lower. Thus, the changes in vapor

410   pressures with the ambient temperature and/or particulate OM loadings might not be

411   the main factors driving gas-particle partitioning of polyol tracers in Nanjing. In

412   Figure 3, the average $F\%$ uncertainties (6.16–31.2%) of monosaccharides (e.g.,

413   fructose) and sugar alcohols (e.g., mannitol) were larger than those of isoprene SOA

414   tracers and levoglucosan (3.33–7.24%) due to their low and variable recoveries (Table

415   S2) and excessive breakthrough (Figure S2). However, the estimated uncertainties of

416   $F\%$ for less volatile polyols ($p^{o,*}_L < \sim 10^{-10}$ atm) were not physically meaningful, as

417   more than 95% of these compounds existed in the particle phase. Considering the

418   uncertainties in $F\%$ and log $p^{o,*}_L$ and high average $F\%$ ($> 85\%$) of target polyol

419   tracers, a dependence of $F\%$ on the vapor pressure could not be determined, and the

420   seasonality and day-night difference ($p > 0.05$) of $F\%$ were obscured.

421   *3.4 Partitioning coefficients of gas versus organic phases*

422   To understand if particulate OM is the only absorbing phase in aerosols for

423   polyol tracers in Nanjing, the absorptive partitioning coefficients of gas vs. organic

424   phases were calculated based on measurement results ($K^m_{p,OM}$) for predefined *Cases*

425   *1-3* and predicted theoretically ($K^t_{p,OM}$) using eq. 3 and vapor pressures listed in Table

426   S4. In Table 1, $K^t_{p,OM}$ ranges of isoprene SOA tracers, levoglucosan, and meso-

427   erythritol are within two orders of magnitude, while those of monosaccharides and

428   mannitol are larger ($> 10^3$).When particulate OM was assumed as the only absorbing

429   phase (*Case 1*), the average $K^m_{p,OM}$ of isoprene SOA tracers, levolgucosan, and meso-

430   erythritol were more than 10 times greater than most of their $K^t_{p,OM}$ (Table 1), and this

431   difference was not likely susceptible to measurement uncertainties. As shown in Table

432   S5, the average relative uncertainties of measurement-based partitioning coefficients

433   are all <50%, leading to an uncertainty of log $K^m_{p,OM}$ less than $\pm$ 0.30. Comparable or

434   even greater (up to 10^5) gap between $K^m_{p,OM}$ and $K^t_{p,OM}$ has been observed for

carbonyls in a number of laboratory and field studies (Healy et al., 2008; Zhao et al., 2013; Shen et al., 2018), which could be ascribed to reactive uptake (e.g., hydration, oligomerization, and esterification) of organic gases onto condensed phase (Galloway et al., 2009). Oligomers, sulfate and nitrate esters of 2-methyltetrols can be formed in the aerosol phase (Surratt et al., 2010; Lin et al., 2014), and their decomposition and hydrolysis during filter analysis will lead to an overestimation of particle-phase concentrations (Lin et al., 2013; Cui et al., 2018). However, the occurrence of oligomers, sulfate or nitrate esters of levoglucosan was not ever reported in ambient aerosols, although it can be readily oxidized by •OH in the aqueous phase of atmospheric particles (Hennigan et al., 2010; Hoffmann et al., 2010).

When solubility in aerosol liquid water was considered by assuming a LLPS in ambient aerosols, and whenever WSOM and WIOM partitioned into separate (*Case 2*) or single (*Case 3*) liquid phases, the average log $K^m_{p,OM}$ of the above mentioned compounds became much closer to or even lay within the range (e.g., levoglucosan) of log $K^t_{p,OM}$ (Table 1). These results indicated that the aerosol liquid water (21.3 ± 24.2 µg m^{-3}; Table S1) is also an important absorbing phase of ambient polyol tracers in Nanjing. Similarly, the measured average *F*% of isoprene SOA tracers in southeastern US and central Amazonia were higher than predictions by assuming instantaneous equilibrium between the gas phase and particulate OM only, and the agreement was improved when parameterization of solubility was included for predictions (Isaacman-VanWertz et al., 2016). But none of these two studies could reasonably predict the temporal variability of *F*% or log $K^m_{p,OM}$. One possible explanation is that the activity coefficients of isoprene SOA tracers and levoglucosan deviate from unity (0.42–2.04; Pye et al., 2018) and vary with PM composition. Pye

459 et al. (2018) re-analyzed the measurement data from Isaacman-VanWertz et al. (2016)

460 using a thermodynamic equilibrium gas-particle partitioning model in two LLPS

461 modes, which involved organic-inorganic interactions and estimations of activity

462 coefficients as a function of liquid PM mixture composition. The resulting predictions

463 captured both the average and diurnal variations of measured $F\%$ for polyol tracers,

464 suggesting a necessity in obtaining time-resolved activity coefficients for the

465 implementation of absorptive equilibrium partitioning model.

466   Unlike isoprene SOA tracers and levoglucosan, the average $K^{t}_{p,OM}$ values of

467 monosaccharides (fructose, mannose, and glucose) and sugar alcohols (xylitol,

468 arabitol, and mannitol) were orders of magnitude larger than their $K^{m}_{p,OM}$ for *Cases 2*

469 *and 3* (Table 1). This is probably caused by the overestimation of gas-phase

470 concentrations of sugar polyols. The organic matter on Q_b is mainly composed of

471 volatile and semi-volatile organic compounds. If the concentrations of organic

472 compounds on Q_b were comparable or higher than those on Q_f, their Q_f values should

473 be dominated by positive artifact. As the vapor pressure decreases, the evaporation

474 loss from Q_f samples becomes non-negligible. Note that the magnitude of negative

475 artifacts is unknown and very difficult to assess, and the vapor pressures of

476 monosaccharides and sugar alcohols are far below 10^{-10} atm (Table S4), their

477 concentrations in Q_b and even PUF samples might contain more contributions from

478 negative artifacts than isoprene SOA tracers and levoglucosan. As low-volatile sugar

479 polyols had lower and less stable recoveries (Table S2) and greater breakthrough

480 (Figure S2e, f), caution is warranted in analyzing their $K^{m}_{p,OM}$ values obtained in this

481 study.

482 *3.5 Partitioning coefficients of gas versus aqueous phases*

483   The predicted Henery's law coefficients in pure water ($K^t_{H,w}$, mol m^{-3} atm^{-1})

484   from EPI and SPARC estimates differed by several orders of magnitude, but literature

485   values of isoprene SOA and levoglucosan were closer to EPI estimates (Table S4). If

486   SPARC $K^*_{H,w}$ values were used, the average log $K^m_{H,e}$ of most polyol tracers would be

487   lower than their average log $K^t_{H,w}$ (Table 2), indicating that the aqueous phase of

488   ambient aerosol is less hospital to polyol tracers than pure water. This is in conflict

489   with the fact that the interactions of organic compounds, water, and inorganic ions in

490   aerosols will increase the partitioning of highly oxygenated compounds (O:C $\geqslant$ 0.6;

491   e.g., isoprene SOA tracers and levoglucosan) into the particle phase (Pye et al., 2018).

492   Several studies identified a close relationship between salt concentrations of aerosol

493   water and enhanced uptake of very polar compounds (Almeida et al., 1983; Kroll et

494   al., 2005; Ip et al., 2009; Kampf et al., 2013; Shen et al., 2018). Thus, log $K^t_{H,w}$ values

495   of EPI estimates were used for further data analysis.

496   In Table 2, the $K^t_{H,w}$ values of isoprene SOA tracers, levoglucosan, and meso-

497   erythritols based on EPI estimations were 10^2 to 10^6 lower than their corresponding

498    $K^m_{H,e}$. Log $K^m_{H,e}$ values of *Cases 2* and *3* had ignorable difference and were not

499   presented separately. Other polyol compounds exhibited less difference between log

500    $K^m_{H,e}$ and log $K^t_{H,w}$, which was very likely caused by the overestimation of their gas-

501   phase concentrations. The average $K^m_{H,e}$ values of polyol tracers (10^{13}–10^{15} mol m^{-3}

502   atm^{-1}) in this study were several orders of magnitude larger than those of carbonyls

503   derived from ambient measurements (10^{10}–10^{12} mol m^{-3} atm^{-1}; Shen et al., 2018) and

504   chamber simulations (~10^{11} mol m^{-3} atm^{-1}; Kroll et al., 2005; Volkamer et al., 2006;

505   Galloway et al., 2009). This is because low molecular weight carbonyls (e.g., glyoxal)

506   are much more volatile ($p^{o,*}_L > 10^{-2}$ atm) than our target polyols (Table S4).

507   According to existing studies, the minimum concentrations of gas-phase glyoxal and

508   methylglyoxal in Chinese cities (~0.1 µg m^{-3}) are magnitudes higher than the averages

509   of polyol tracers in this work, while their particle-phase concentrations are of the

510   same magnitude (Shen et al., 2018; Liu et al., 2020).

511   A number of previous studies observed enhanced $K_{H,e}$ of carbonyls with salt

512   concentrations in aqueous solution (Ip et al., 2009; Kampf et al., 2013; Waxman et al.,

513   2015; Shen et al., 2018), and described this "salting-in" effect using

514    $\text{Log}\left(\dfrac{K_{H,w}}{K_{H,e}}\right) = K_s c_{salt}$ (7)

515   where K_s (kg mol^{-1}) is the salting constant, and c_{salt} is the aqueous-phase concentration

516   of salt in mol kg^{-1} ALWC. This equation is originally defined in Setschenow (1889)

517   by plotting log ($K_{H,w}/K_{H,e}$) versus the total salt concentration (mol L^{-1}).

518   As sulfate has been identified as the major factor influencing the salting effect of

519   carbonyl species (Kroll et al., 2005; Ip et al., 2009), Figure 4 shows modified

520   Setschenow plots for C5-alkene triols, 2-methyltetrols, and levoglucosan, where log

521   ($K^t_{H,w}/K^m_{H,e}$) values were regressed to the molality of sulfate ion in aerosol liquid

522   water ($c_{sulfate}$, mol kg^{-1} ALWC). The log ($K^t_{H,w}/K^m_{H,e}$) data increased faster when $c_{sulfate}$

523   approached 0, and deviated from their expected behavior with increased $c_{sulfate}$. Kampf

524   et al. (2013) selected a threshold $c_{sulfate}$ of 12 mol kg^{-1} ALWC to illustrate the

525   deviation for chamber experiments, and attributed it to elevated viscosity and slow

526   particle-phase reactions at high $c_{sulfate}$. In Figure 4, negative correlations ($p < 0.01$) are

527   observed at $c_{sulfate} < 12$ mol kg^{-1} ALWC, and Figure S5 exhibits significant negative

528   correlations ($p < 0.01$) between log ($K^t_{H,w}/K^m_{H,e}$) and $c_{sulfate}$ for individual polyols even

529   without excluding the deviations at high $c_{sulfate}$. The K_s values of polyol tracers from

530   Figures 4 and S5 (-0.17 – -0.037 kg mol^{-1}) are in a similar range as that of glyoxal (-

531 0.24 – -0.04 kg mol^{-1}; Kampf et al., 2013; Shen et al., 2018; Waxman et al., 2015).

532 These results indicated that the shifting of gas-particle equilibrium toward the

533 condensed phase might be partly parameterized by the equation defining "salting-in"

534 effects.

535   However, the "salting-in" effect is a known phenomenon that is not likely linked

536 with a specific physical or chemical mechanism. Quantum chemical calculation

537 results indicated negative Gibbs free energy of water displacement for interactions

538 between SO_4^{2-} and glyoxal monohydrate (Waxman et al., 2015). The net "salting-in"

539 effect of 1-nitro-2-naphthol in NaF solution was interpreted by postulating hydrogen

540 bonding (Almeida et al., 1983). A direct binding of cations to ether oxygens was

541 proposed to be responsible for the increased solubility of water-soluble polymers

542 (Sadeghi and Jahani, 2012). Due to the moderate correlations and negative intercepts

543 in Figures 4 and S5, the gap between $K^t_{H,e}$ and $K^m_{H,w}$ cannot be closed by the "salting-

544 in" effect alone. Shen et al. (2018) also obtained negative intercepts when plotting log

545 ($K^t_{H,w}/K^m_{H,e}$) over $c_{sulfate}$ for glyoxal and methylglyoxal in ambient atmosphere, and

546 attributed this to unknown gas-particle partitioning mechanisms. There is evidence

547 showing that conventional GC/EI-MS analysis overestimates particle-phase 2-

548 methyltetrols by 60-188% due (in part) to the thermal degradation of less volatile

549 oligomers and organosulfates (Cui et al., 2018). To fit the gas-particle distribution of

550 2-methyltetrols in southeastern US, 50% of particulate 2-methyltetrols was presumed

551 to exist in chemical forms with much lower vapor pressures by Pye et al. (2018). So,

552 the reactive uptake and aqueous phase chemistry could be explanations for the

553 enhanced uptake of isoprene SOA tracers. Moreover, log ($K^t_{H,w}/K^m_{H,e}$) values of

554 polyol tracers also negatively correlated with the aqueous-phase concentrations of

555 WSOC (c_{WSOC}, Figure S6), but not NH_4^+ or NO_3^-. This dependence might be

556 associated with the "like-dissolves-like" rule, or indicate the importance of aqueous-

557 phase heterogeneous reactions (Hennigan et al., 2009; Volkamer et al., 2009).

558 Although several studies have estimated Henry's law constants for a variety of polar

559 organic compounds in pure water (e.g., polyols and polyacids; Compernolle and

560 Müller, 2014a, b), more work is warranted to decrease the estimation uncertainty and

561 explain their increased partitioning toward aerosol liquid water explicitly.

4 Implications and conclusions

563 In this work, concentrations of gas- and particle-phase polyol tracers were

564 measured simultaneously in northern Nanjing. The temporal variations of individual

565 compounds were dominated by their particle-phase concentrations. Then gas-particle

566 partitioning of polyol tracers should have little influence on source apportionment

567 based on particle-phase data in Nanjing. An improved agreement between

568 measurement-based and predicted $K_{p,OM}$ of polyol tracers was observed when the

569 solubility in aerosol liquid water was considered, indicating that the aqueous solution

570 in aerosols is also an important absorbing phase. The large gaps of $K^m_{H,e}$ versus $K^t_{H,w}$

571 could be partly parameterized using the equation defining "salting-in" effects.

572 According to existing studies, reactive uptake, aqueous phase reactions, and chemical

573 similarity between partitioning species and the absorbing phase might be responsible

574 for increasing the partitioning of polyol tracers into the condensed phase. So, the

575 results of this study have important implications on the prediction of gas-particle

576 partitioning of water-soluble organics, and further studies are required to explain their

577 enhanced aqueous-phase uptake mechanistically. Due to the hygroscopic properties of

578 highly oxidized organic aerosols, this study also partly reveals the discrepancy

579 between modeled and observed SOA in previous studies. However, several

580 assumptions (e.g., LLPS) were made for proposed gas-particle partitioning schemes in

581 this work, more laboratory research is needed to understand the mixing state of

582 inorganic salts, organic components, and aerosol liquid water in atmospheric particles.

583

584 *Data availability*

585 Data used in the writing of this paper is available at the Harvard Dataverse

586 (https://doi.org/10.7910/DVN/U3IGQR, Qin et al., 2021)

587

588 *Author contributions*

589 MX designed the research. CQ and YG performed the sampling and chemical analysis.

590 CQ, YM, and MX analyzed the data. CQ and MX wrote the paper with significant

591 contributions from YW, HL, and QW.

592

593 *Competing interests*

594 The authors declare that they have no conflict of interest.

595

596 *Acknowledgements*

597 This research was supported by the National Natural Science Foundation of China

598 (NSFC, 41701551), Postdoctoral Research Foundation of China (2020M671519), and

599 the Fundamental Research Funds for the Central Universities (KJQN202122). Y. W.

600 was supported by the National Science Foundation Atmospheric Chemistry Program.

601

602

References

Ahrens, L., Shoeib, M., Harner, T., Lane, D. A., Guo, R., and Reiner, E. J.: Comparison of annular diffusion denuder and high volume air samplers for measuring per- and polyfluoroalkyl substances in the atmosphere, Anal. Chem., 83, 9622-9628, 10.1021/ac202414w, 2011.

Almeida, M. B., Alvarez, A. M., Miguel, E. M. D., and Hoyo, E. S. D.: Setchenow coefficients for naphthols by distribution method, Can. J. Chem., 61, 244-248, 10.1139/v83-043, 1983.

Barsanti, K. C., and Pankow, J. F.: Thermodynamics of the formation of atmospheric organic particulate matter by accretion reactions—Part 1: aldehydes and ketones, Atmos. Environ., 38, 4371-4382, 10.1016/j.atmosenv.2004.03.035, 2004.

Bauer, H., Claeys, M., Vermeylen, R., Schueller, E., Weinke, G., Berger, A., and Puxbaum, H.: Arabitol and mannitol as tracers for the quantification of airborne fungal spores, Atmos. Environ., 42, 588-593, https://doi.org/10.1016/j.atmosenv.2007.10.013, 2008.

Burshtein, N., Lang-Yona, N., and Rudich, Y.: Ergosterol, arabitol and mannitol as tracers for biogenic aerosols in the eastern Mediterranean, Atmos. Chem. Phys., 11, 829-839, 10.5194/acp-11-829-2011, 2011.

Claeys, M., Graham, B., Vas, G., Wang, W., Vermeylen, R., Pashynska, V., Cafmeyer, J., Guyon, P., Andreae, M. O., Artaxo, P., and Maenhaut, W.: Formation of secondary organic aerosols through photooxidation of isoprene, Science, 303, 1173-1176, 10.1126/science.1092805, 2004.

Compernolle, S., and Müller, J. F.: Henry's law constants of polyols, Atmos. Chem. Phys., 14, 12815-12837, 10.5194/acp-14-12815-2014, 2014a.

Compernolle, S., and Müller, J. F.: Henry's law constants of diacids and hydroxy polyacids: recommended values, Atmos. Chem. Phys., 14, 2699-2712, 10.5194/acp-14-2699-2014, 2014b.

Cui, T., Zeng, Z., dos Santos, E. O., Zhang, Z., Chen, Y., Zhang, Y., Rose, C. A., Budisulistiorini, S. H., Collins, L. B., Bodnar, W. M., de Souza, R. A. F., Martin, S. T., Machado, C. M. D., Turpin, B. J., Gold, A., Ault, A. P., and Surratt, J. D.: Development of a hydrophilic interaction liquid chromatography (HILIC) method for the chemical characterization of water-soluble isoprene epoxydiol (IEPOX)-derived secondary organic aerosol, Environmental Science: Environ. Sci.: Process. Impacts, 20, 1524-1536, 10.1039/C8EM00308D, 2018.

Fu, P., and Kawamura, K.: Diurnal variations of polar organic tracers in summer forest aerosols: A case study of a Quercus and Picea mixed forest in Hokkaido, Japan, Geochem. J., 45, 297-308, 10.2343/geochemj.1.0123, 2011.

Galloway, M. M., Chhabra, P. S., Chan, A. W. H., Surratt, J. D., Flagan, R. C., Seinfeld, J. H., and Keutsch, F. N.: Glyoxal uptake on ammonium sulphate seed aerosol: reaction products and reversibility of uptake under dark and irradiated conditions, Atmos. Chem. Phys., 9, 3331-3345, 10.5194/acp-9-3331-2009, 2009.

Hallar, A. G., Lowenthal, D. H., Clegg, S. L., Samburova, V., Taylor, N., Mazzoleni, L. R., Zielinska, B. K., Kristensen, T. B., Chirokova, G., McCubbin, I. B., Dodson, C., and Collins, D.: Chemical and hygroscopic properties of aerosol organics at Storm Peak Laboratory, J. Geophys. Res. Atmos., 118, 4767-4779, https://doi.org/10.1002/jgrd.50373, 2013.

Heald, C. L., Jacob, D. J., Park, R. J., Russell, L. M., Huebert, B. J., Seinfeld, J. H., Liao, H., and Weber, R. J.: A large organic aerosol source in the free troposphere missing from current models, Geophys. Res. Lett., 32, L18809, https://doi.org/10.1029/2005GL023831, 2005.

Healy, R. M., Wenger, J. C., Metzger, A., Duplissy, J., Kalberer, M., and Dommen, J.: Gas/particle partitioning of carbonyls in the photooxidation of isoprene and 1,3,5-trimethylbenzene, Atmos. Chem. Phys., 8, 3215-3230, 10.5194/acp-8-3215-2008, 2008.

Hennigan, C. J., Bergin, M. H., Russell, A. G., Nenes, A., and Weber, R. J.: Gas/particle partitioning of water-soluble organic aerosol in Atlanta, Atmos. Chem. Phys., 9, 3613-3628, 10.5194/acp-9-3613-2009, 2009.

Hennigan, C. J., Sullivan, A. P., Collett Jr, J. L., and Robinson, A. L.: Levoglucosan stability in biomass burning particles exposed to hydroxyl radicals, Geophys. Res. Lett., 37, L09806, https://doi.org/10.1029/2010GL043088, 2010.

Hilal, S. H., Ayyampalayam, S. N., and Carreira, L. A.: Air−liquid partition coefficient for a diverse set of organic compounds: Henry's Law constant in water and hexadecane, Environ. Sci. Technol., 42, 9231-9236, 10.1021/es8005783, 2008.

Hodzic, A., Jimenez, J. L., Madronich, S., Canagaratna, M. R., DeCarlo, P. F., Kleinman, L., and Fast, J.: Modeling organic aerosols in a megacity: potential contribution of semi-volatile and intermediate volatility primary organic compounds to secondary organic aerosol formation,

Atmos. Chem. Phys., 10, 5491-5514, 10.5194/acp-10-5491-2010, 2010.

Hoffmann, D., Tilgner, A., Iinuma, Y., and Herrmann, H.: Atmospheric stability of levoglucosan: A detailed laboratory and modeling study, Environ. Sci. Technol., 44, 694-699, 10.1021/es902476f, 2010.

Hu, D., Bian, Q., Lau, A. K. H., and Yu, J. Z.: Source apportioning of primary and secondary organic carbon in summer PM2.5 in Hong Kong using positive matrix factorization of secondary and primary organic tracer data, J. Geophys. Res. Atmos., 115, D16204, https://doi.org/10.1029/2009JD012498, 2010.

Ip, H. S. S., Huang, X. H. H., and Yu, J. Z.: Effective Henry's law constants of glyoxal, glyoxylic acid, and glycolic acid, Geophys. Res. Lett., 36, L01802, https://doi.org/10.1029/2008GL036212, 2009.

Isaacman-VanWertz, G., Yee, L. D., Kreisberg, N. M., Wernis, R., Moss, J. A., Hering, S. V., de Sá, S. S., Martin, S. T., Alexander, M. L., Palm, B. B., Hu, W., Campuzano-Jost, P., Day, D. A., Jimenez, J. L., Riva, M., Surratt, J. D., Viegas, J., Manzi, A., Edgerton, E., Baumann, K., Souza, R., Artaxo, P., and Goldstein, A. H.: Ambient gas-particle partitioning of tracers for biogenic oxidation, Environ. Sci. Technol., 50, 9952-9962, 10.1021/acs.est.6b01674, 2016.

Jang, M., Czoschke, N. M., Lee, S., and Kamens, R. M.: Heterogeneous atmospheric aerosol production by acid-catalyzed particle-phase reactions, Science, 298, 814, 10.1126/science.1075798, 2002.

Kampf, C. J., Waxman, E. M., Slowik, J. G., Dommen, J., Pfaffenberger, L., Praplan, A. P., Prévôt, A. S. H., Baltensperger, U., Hoffmann, T., and Volkamer, R.: Effective Henry's law partitioning and the salting constant of glyoxal in aerosols containing sulfate, Environ. Sci. Technol., 47, 4236-4244, 10.1021/es400083d, 2013.

Kondo, Y., Miyazaki, Y., Takegawa, N., Miyakawa, T., Weber, R. J., Jimenez, J. L., Zhang, Q., and Worsnop, D. R.: Oxygenated and water-soluble organic aerosols in Tokyo, J. Geophys. Res. Atmos., 112, D01203, 10.1029/2006jd007056, 2007.

Kroll, J. H., Ng, N. L., Murphy, S. M., Varutbangkul, V., Flagan, R. C., and Seinfeld, J. H.: Chamber studies of secondary organic aerosol growth by reactive uptake of simple carbonyl compounds, J. Geophys. Res. Atmos., 110, D23207, https://doi.org/10.1029/2005JD006004, 2005.

Liang, C., and Pankow, J. F.: Gas/particle partitioning of organic compounds to environmental tobacco smoke: Partition coefficient measurements by desorption and comparison to urban particulate material, Environ. Sci. Technol., 30, 2800-2805, 10.1021/es960050x, 1996.

Liang, C., Pankow, J. F., Odum, J. R., and Seinfeld, J. H.: Gas/particle partitioning of semivolatile organic compounds to model inorganic, organic, and ambient smog aerosols, Environ. Sci. Technol., 31, 3086-3092, 10.1021/es9702529, 1997.

Lin, Y.-H., Budisulistiorini, S. H., Chu, K., Siejack, R. A., Zhang, H., Riva, M., Zhang, Z., Gold, A., Kautzman, K. E., and Surratt, J. D.: Light-absorbing oligomer formation in secondary organic aerosol from reactive uptake of isoprene epoxydiols, Environ. Sci. Technol., 48, 12012-12021, 10.1021/es503142b, 2014.

Lin, Y. H., Knipping, E. M., Edgerton, E. S., Shaw, S. L., and Surratt, J. D.: Investigating the influences of SO2 and NH3 levels on isoprene-derived secondary organic aerosol formation using conditional sampling approaches, Atmos. Chem. Phys., 13, 8457-8470, 10.5194/acp-13-8457-2013, 2013.

Liu, J., Li, X., Li, D., Xu, R., Gao, Y., Chen, S., Liu, Y., Zhao, G., Wang, H., Wang, H., Lou, S., Chen, M., Hu, J., Lu, K., Wu, Z., Hu, M., Zeng, L., and Zhang, Y.: Observations of glyoxal and methylglyoxal in a suburban area of the Yangtze River Delta, China, Atmos. Environ., 238, 117727, https://doi.org/10.1016/j.atmosenv.2020.117727, 2020.

Mader, B. T., and Pankow, J. F.: Study of the effects of particle-phase carbon on the gas/particle partitioning of semivolatile organic compounds in the atmosphere using controlled field experiments, Environ. Sci. Technol., 36, 5218-5228, 10.1021/es011048v, 2002.

Odum, J. R., Hoffmann, T., Bowman, F., Collins, D., Flagan, R. C., and Seinfeld, J. H.: Gas/particle partitioning and secondary organic aerosol yields, Environ. Sci. Technol., 30, 2580-2585, 10.1021/es950943+, 1996.

Pankow, J. F.: An absorption model of the gas/aerosol partitioning involved in the formation of secondary organic aerosol, Atmos. Environ., 28, 189-193, 10.1016/1352-2310(94)90094-9, 1994a.

Pankow, J. F.: An absorption model of gas/particle partitioning of organic compounds in the atmosphere, Atmos. Environ., 28, 185-188, 10.1016/1352-2310(94)90093-0, 1994b.

Perraud, V., Bruns, E. A., Ezell, M. J., Johnson, S. N., Yu, Y., Alexander, M. L., Zelenyuk, A., Imre, D., Chang, W. L., Dabdub, D., Pankow, J. F., and Finlayson-Pitts, B. J.: Nonequilibrium

atmospheric secondary organic aerosol formation and growth, Proc. Natl. Acad. Sci. U.S.A., 109, 2836-2841, 10.1073/pnas.1119909109, 2012.

Peters, A. J., Lane, D. A., Gundel, L. A., Northcott, G. L., and Jones, K. C.: A comparison of high volume and diffusion denuder samplers for measuring semivolatile organic compounds in the atmosphere, Environ. Sci. Technol., 34, 5001-5006, 10.1021/es000056t, 2000.

Pye, H. O. T., Zuend, A., Fry, J. L., Isaacman-VanWertz, G., Capps, S. L., Appel, K. W., Foroutan, H., Xu, L., Ng, N. L., and Goldstein, A. H.: Coupling of organic and inorganic aerosol systems and the effect on gas–particle partitioning in the southeastern US, Atmos. Chem. Phys., 18, 357-370, 10.5194/acp-18-357-2018, 2018.

Qin, C., Gou, Y., Wang, Y., Mao, Y., Liao, H., Wang, Q. g., and Xie, M.: Replication Data for: Gas-particle partitioning of polyol tracers in the western Yangtze River Delta, China, in, V2 ed., Harvard Dataverse, https://doi.org/10.7910/DVN/U3IGQR, 2021.

Sadeghi, R., and Jahani, F.: Salting-in and salting-out of water-soluble polymers in aqueous salt solutions, J. Phys. Chem. B, 116, 5234-5241, 10.1021/jp300665b, 2012.

Saxena, P., and Hildemann, L.: Water-soluble organics in atmospheric particles: A critical review of the literature and application of thermodynamics to identify candidate compounds, J. Atmos. Chem., 24, 57-109, 10.1007/bf00053823, 1996.

Setschenow, J.: Über die Konstitution der Salzlösungen auf Grund ihres Verhaltens zu Kohlensäure, Z. Phys. Chem., 4U, 117-125, https://doi.org/10.1515/zpch-1889-0409, 1889.

Shen, H., Chen, Z., Li, H., Qian, X., Qin, X., and Shi, W.: Gas-particle partitioning of carbonyl compounds in the ambient atmosphere, Environ. Sci. Technol., 52, 10997-11006, 10.1021/acs.est.8b01882, 2018.

Simcik, M. F., Franz, T. P., Zhang, H., and Eisenreich, S. J.: Gas-particle partitioning of PCBs and PAHs in the Chicago urban and adjacent coastal atmosphere: States of equilibrium, Environ. Sci. Technol., 32, 251-257, 10.1021/es970557n, 1998.

Simoneit, B. R. T., Schauer, J. J., Nolte, C. G., Oros, D. R., Elias, V. O., Fraser, M. P., Rogge, W. F., and Cass, G. R.: Levoglucosan, a tracer for cellulose in biomass burning and atmospheric particles, Atmos. Environ., 33, 173-182, http://dx.doi.org/10.1016/S1352-2310(98)00145-9, 1999.

Simoneit, B. R. T., Elias, V. O., Kobayashi, M., Kawamura, K., Rushdi, A. I., Medeiros, P. M., Rogge, W. F., and Didyk, B. M.: Sugars dominant water-soluble organic compounds in soils and characterization as tracers in atmospheric particulate matter, Environ. Sci. Technol., 38, 5939-5949, 10.1021/es0403099, 2004.

Surratt, J. D., Murphy, S. M., Kroll, J. H., Ng, N. L., Hildebrandt, L., Sorooshian, A., Szmigielski, R., Vermeylen, R., Maenhaut, W., Claeys, M., Flagan, R. C., and Seinfeld, J. H.: Chemical composition of secondary organic aerosol formed from the photooxidation of isoprene, J. Phys. Chem. A, 110, 9665-9690, 10.1021/jp061734m, 2006.

Surratt, J. D., Chan, A. W. H., Eddingsaas, N. C., Chan, M., Loza, C. L., Kwan, A. J., Hersey, S. P., Flagan, R. C., Wennberg, P. O., and Seinfeld, J. H.: Reactive intermediates revealed in secondary organic aerosol formation from isoprene, Proc. Natl. Acad. Sci. U.S.A., 107, 6640-6645, 10.1073/pnas.0911114107, 2010.

Taylor, N. F., Collins, D. R., Lowenthal, D. H., McCubbin, I. B., Hallar, A. G., Samburova, V., Zielinska, B., Kumar, N., and Mazzoleni, L. R.: Hygroscopic growth of water soluble organic carbon isolated from atmospheric aerosol collected at US national parks and Storm Peak Laboratory, Atmos. Chem. Phys., 17, 2555-2571, 10.5194/acp-17-2555-2017, 2017.

Tsyro, S. G.: To what extent can aerosol water explain the discrepancy between model calculated and gravimetric PM10 and PM2.5?, Atmos. Chem. Phys., 5, 515-532, 10.5194/acp-5-515-2005, 2005.

Turpin, B. J., and Lim, H.-J.: Species contributions to PM2.5 mass concentrations: Revisiting common assumptions for estimating organic mass, Aerosol Sci. Technol., 35, 602-610, 10.1080/02786820119445, 2001.

US EPA: Estimation Program Interface (EPI) Suite. Version v4.11, 2012. United States Environmental Protection Agency, Washington, DC, USA. https://www.epa.gov/tsca-screening-tools/download-epi-suitetm-estimation-program-interface-v411

Volkamer, R., Jimenez, J. L., San Martini, F., Dzepina, K., Zhang, Q., Salcedo, D., Molina, L. T., Worsnop, D. R., and Molina, M. J.: Secondary organic aerosol formation from anthropogenic air pollution: Rapid and higher than expected, Geophys. Res. Lett., 33, L17811, https://doi.org/10.1029/2006GL026899, 2006.

Volkamer, R., Ziemann, P. J., and Molina, M. J.: Secondary Organic Aerosol Formation from Acetylene (C2H2): seed effect on SOA yields due to organic photochemistry in the aerosol

776   aqueous phase, Atmos. Chem. Phys., 9, 1907-1928, 10.5194/acp-9-1907-2009, 2009.

777 Wang, W., Kourtchev, I., Graham, B., Cafmeyer, J., Maenhaut, W., and Claeys, M.: Characterization
778   of oxygenated derivatives of isoprene related to 2-methyltetrols in Amazonian aerosols using
779   trimethylsilylation and gas chromatography/ion trap mass spectrometry, Rapid Commun. Mass
780   Spectrom., 19, 1343-1351, https://doi.org/10.1002/rcm.1940, 2005.

781 Waxman, E. M., Elm, J., Kurtén, T., Mikkelsen, K. V., Ziemann, P. J., and Volkamer, R.: Glyoxal and
782   methylglyoxal Setschenow salting constants in sulfate, nitrate, and chloride solutions:
783   Measurements and Gibbs energies, Environ. Sci. Technol., 49, 11500-11508,
784   10.1021/acs.est.5b02782, 2015.

785 Williams, B. J., Goldstein, A. H., Kreisberg, N. M., and Hering, S. V.: In situ measurements of
786   gas/particle-phase transitions for atmospheric semivolatile organic compounds, Proc. Natl. Acad.
787   Sci. U.S.A., 107, 6676-6681, 10.1073/pnas.0911858107, 2010.

788 Xie, M., Barsanti, K. C., Hannigan, M. P., Dutton, S. J., and Vedal, S.: Positive matrix factorization of
789   PM2.5 - eliminating the effects of gas/particle partitioning of semivolatile organic compounds,
790   Atmos. Chem. Phys., 13, 7381-7393, 10.5194/acp-13-7381-2013, 2013.

791 Xie, M., Hannigan, M. P., and Barsanti, K. C.: Gas/particle partitioning of n-alkanes, PAHs and
792   oxygenated PAHs in urban Denver, Atmos. Environ., 95, 355-362,
793   http://dx.doi.org/10.1016/j.atmosenv.2014.06.056, 2014a.

794 Xie, M., Hannigan, M. P., and Barsanti, K. C.: Gas/particle partitioning of 2-methyltetrols and
795   levoglucosan at an urban site in Denver, Environ. Sci. Technol., 48, 2835-2842,
796   10.1021/es405356n, 2014b.

797 Xie, M., Hannigan, M. P., and Barsanti, K. C.: Impact of gas/particle partitioning of semivolatile
798   organic compounds on source apportionment with positive matrix factorization, Environ. Sci.
799   Technol., 48, 9053-9060, 10.1021/es5022262, 2014c.

800 Yang, L., Shang, Y., Hannigan, M. P., Zhu, R., Wang, Q. g., Qin, C., and Xie, M.: Collocated
801   speciation of PM2.5 using tandem quartz filters in northern nanjing, China: Sampling artifacts and
802   measurement uncertainty, Atmos. Environ., 246, 118066,
803   https://doi.org/10.1016/j.atmosenv.2020.118066, 2021.

804 Yatavelli, R. L. N., Stark, H., Thompson, S. L., Kimmel, J. R., Cubison, M. J., Day, D. A.,
805   Campuzano-Jost, P., Palm, B. B., Hodzic, A., Thornton, J. A., Jayne, J. T., Worsnop, D. R., and
806   Jimenez, J. L.: Semicontinuous measurements of gas–particle partitioning of organic acids in a
807   ponderosa pine forest using a MOVI-HRToF-CIMS, Atmos. Chem. Phys., 14, 1527-1546,
808   10.5194/acp-14-1527-2014, 2014.

809 Zhang, Y., Sheesley, R. J., Schauer, J. J., Lewandowski, M., Jaoui, M., Offenberg, J. H., Kleindienst, T.
810   E., and Edney, E. O.: Source apportionment of primary and secondary organic aerosols using
811   positive matrix factorization (PMF) of molecular markers, Atmos. Environ., 43, 5567-5574,
812   https://doi.org/10.1016/j.atmosenv.2009.02.047, 2009.

813 Zhao, Y., Kreisberg, N. M., Worton, D. R., Isaacman, G., Weber, R. J., Liu, S., Day, D. A., Russell, L.
814   M., Markovic, M. Z., VandenBoer, T. C., Murphy, J. G., Hering, S. V., and Goldstein, A. H.:
815   Insights into secondary organic aerosol formation mechanisms from measured gas/particle
816   partitioning of specific organic tracer compounds, Environ. Sci. Technol., 47, 3781-3787,
817   10.1021/es304587x, 2013.

818 Zuend, A., and Seinfeld, J. H.: Modeling the gas-particle partitioning of secondary organic aerosol: the
819   importance of liquid-liquid phase separation, Atmos. Chem. Phys., 12, 3857-3882, 10.5194/acp-
820   12-3857-2012, 2012.

821

Table 1. Comparisons of measurement-based log $K_{p,OM}$ (m^3 µg^{-1}) at three proposed cases and predicted values.

Species	No. of obs.	Log $K^m_{p,OM}$ [a]			Log $K_{p,OM}$ [b]			
		Case 1	Case 2	Case 3	EPI	EVAPORATION	SPARC	SIMPOL
Isoprene SOA tracers								
C5-alkene triol 1	53	0.33 ± 0.71	-0.79 ± 0.86	-0.82 ± 0.85	-3.09	-2.84	-1.19	-2.88
C5-alkene triol 2	63	0.15 ± 0.55	-1.02 ± 0.74	-1.05 ± 0.73	-3.62	-3.67	-4.14	-2.85
C5-alkene triol 3	83	0.35 ± 0.68	-0.83 ± 0.86	-0.86 ± 0.85	-2.90	-2.65	-1.00	-2.69
2-Methylthreitol	101	-0.12 ± 0.48	-2.09 ± 0.71	-2.09 ± 0.70	-1.87	-1.30	-1.18	-0.47
2-Methylerythritol	95	-0.011 ± 0.58	-1.96 ± 0.71	-1.96 ± 0.71	-1.90	-1.34	-1.22	-0.50
Biomass burning tracer								
Levoglucosan	65	2.23 ± 0.72	0.63 ± 0.90	0.62 ± 0.90	-0.04	-0.81	1.04	-0.76
Sugars ang sugar alcohols								
Meso-erythritol	31	0.87 ± 0.53	-1.43 ± 0.60	-1.43 ± 0.60	-0.65	-1.21	-0.45	
Fructose	85	0.65 ± 0.73	-1.20 ± 0.83	-1.20 ± 0.89	1.17	2.76	6.94	
Mannose	74	0.62 ± 0.71	-2.12 ± 0.95	-2.12 ± 0.95	1.28	2.13	4.77	
Glucose	88	0.42 ± 0.67	-2.77 ± 0.93	-2.77 ± 0.93	0.34	3.75	7.32	
Xylitol	22	0.24 ± 0.54	-2.61 ± 0.72	-2.61 ± 0.72	3.37	2.34	3.57	
Arabitol	30	1.46 ± 0.89	-1.35 ± 1.24	-1.35 ± 1.24	3.25	1.67	2.90	
Manitol	65	1.08 ± 0.63	-2.24 ± 0.95	-2.24 ± 0.95	2.33	4.16	6.68	

[a] Logarithms with base 10, average ± standard deviation; [b] temperature range: -4~36 ºC.

Table 2. Comparisons of measurement-based log $K_{H,e}$ (mol m^{-3} atm^{-1}) and predicted log $K_{H,w}$ of individual polyol tracers.

Species	No. of obs.	Log $K^m_{H,e}$ (Cases 2)[a]			Log $K^t_{H,w}$[b]	
		Median	Average	Range	EPI	SPARC
Isoprene SOA tracers						
C5-alkene triol 1	53	14.0	13.9 ± 0.86	11.5 – 16.4	7.22	11.7
C5-alkene triol 2	63	13.7	13.6 ± 0.73	11.2 – 16.1	7.34	7.66
C5-alkene triol 3	83	13.9	13.8 ± 0.85	10.6 – 16.1	7.43	11.9
2-Methylthreitol	101	13.4	13.3 ± 0.70	10.9 – 14.8	10.0	14.1
2-Methylerythritol	95	13.5	13.5 ± 0.71	11.6 – 15.6	9.95	14.1
Biomass burning tracer						
Levoglucosan	65	15.7	15.7 ± 0.90	13.2 – 17.3	13.4	16.1
Sugars ang sugar alcohols						
Meso-erythritol	31	14.5	14.4 ± 0.60	12.8 – 15.6	9.65	13.8
Fructose	85	14.2	14.1 ± 0.89	11.9 – 16.5	14.7	19.9
Mannose	74	14.0	14.1 ± 0.94	12.1 – 16.8	10.9	18.8
Glucose	88	13.9	13.9 ± 0.93	11.3 – 16.3	14.7	20.9
Xylitol	22	13.8	13.7 ± 0.72	12.6 – 15.0	12.1	18.1
Arabitol	30	15.1	15.0 ± 1.23	13.0 – 18.2	11.3	17.4
Mannitol	65	14.6	14.5 ± 0.94	12.1 – 16.4	12.9	20.8

[a] Logarithms with base 10 (log $K^m_{H,e}$ values of *Case 3* had ignorable difference, and were not exhibited separately); [b] temperature range: -4~36 °C.

Figure 1
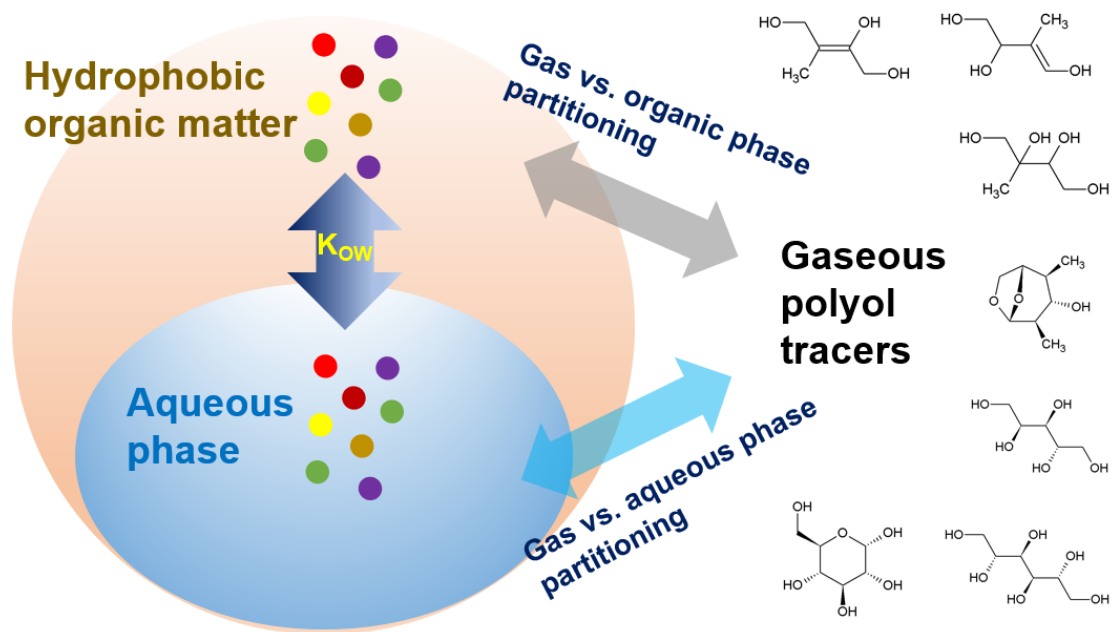
Figure 1. Proposed scheme for gas-particle partitioning of polyol tracers.

Figure 2
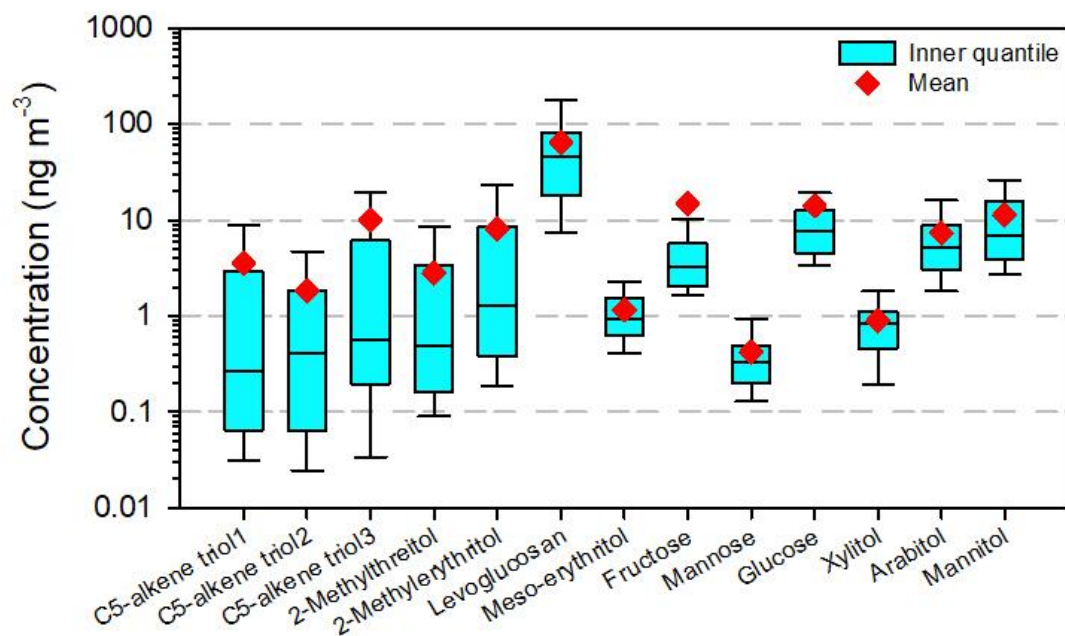
Figure 2. Total concentrations of individual polyols (Q_f + Q_b + PUF) in the ambient atmosphere of northern Nanjing. The boxes depict the median (dark line), inner quantile range (box), 10th and 90th percentiles (whiskers), and the mean (red diamond).

Figure 3
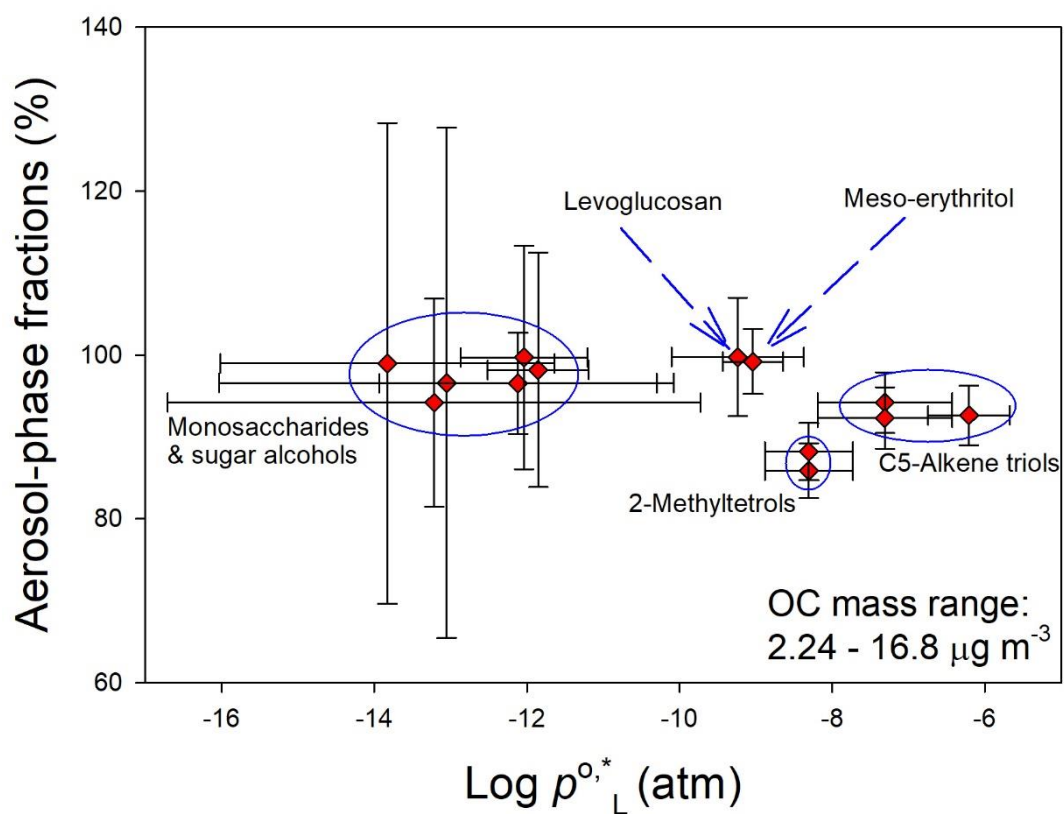
Figure 3. Average particle-phase fractions and log $p^{o,*}_L$ of individual polyol tracers. Whiskers represent uncertainties of $F\%$ and one standard deviation of log $p^{o,*}_L$ derived from different estimation tools.

Figure 4
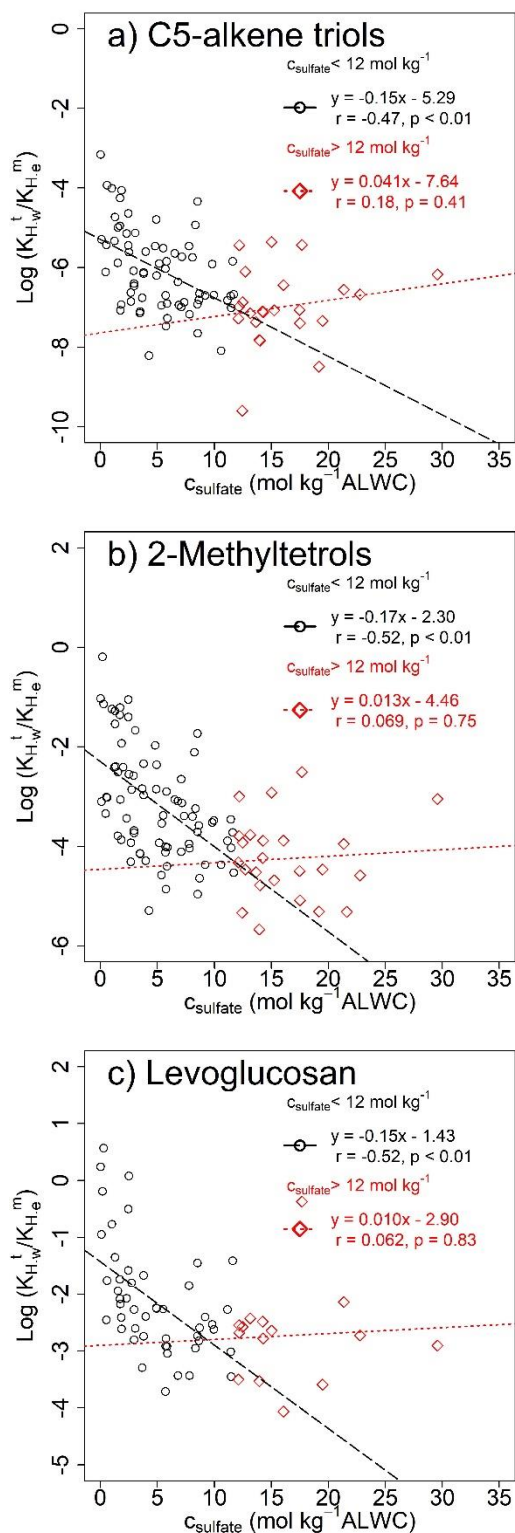
Figure 4. Modified Setschenow plots of log ($K^t_{H,w}/K^m_{H,e}$) versus $c_{sulfate}$ for (a) C5-alkene triols, (b) 2-methyltetrols, and (c) levoglucosan.